

# UNMANNED AERIAL VEHICLES

MEAER

---

## Laboratory 2 - Estimation of Motion Variables of the Parrot AR.Drone

---

### Group 3:

- |                             |  |
|-----------------------------|--|
| 1. João Peixoto, No. 95807  | Signature: <i>João Paulo Martins Peixoto</i> |
| 2. José Bento, No. 95815    | Signature: <i>José Bento</i>                 |
| 3. Thomas Childs, No. 95847 | Signature: <i>Thomas Maurício Childs</i>     |

**Instructor:** Rita Cunha

**2022/2023 – First Semester**

# Contents

<b>1</b>	<b>Introduction and goals</b>	<b>1</b>
<b>2</b>	<b>Setup and experiments</b>	<b>1</b>
<b>3</b>	<b>Modelling and characterisation of the sensors</b>	<b>1</b>
3.1	Statistical characterisation of the measurements <i>A</i> through <i>C</i>	3
3.1.1	<i>Experiment A</i>	3
3.1.2	<i>Experiment B</i>	3
3.1.3	<i>Experiment C</i>	4
3.2	Using the accelerometers as inclinometers	5
<b>4</b>	<b>Kalman Filters</b>	<b>7</b>
4.1	Kalman filter for pitch/roll estimation: design & implementation	7
4.1.1	Pitch	7
4.1.2	Roll	8
4.2	Transfer function	9
4.2.1	Pitch	9
4.2.2	Roll	9
4.3	Parameters Q and R	10
4.4	Including gyro bias as an extra state	11
4.5	Complementary filters	11
4.5.1	Without including gyro bias as extra state	12
4.5.2	Including gyro bias as extra states	13
4.6	Discussion of the results obtained	13
<b>5</b>	<b>Integrated roll and pitch estimation</b>	<b>13</b>
5.1	Observability	14
5.2	Kalman filter design	14
5.3	Validation	15
5.4	Experimental results	16
<b>6</b>	<b>Conclusions</b>	<b>17</b>

# 1 Introduction and goals

This laboratory work concerns the design, implementation and analysis of several estimation solutions for the roll and pitch angles of a quadrotor. As such, there are five main goals to achieve:

- Modelling and characterization of the motion sensors;
- Raw computation of roll and pitch angles;
- Design, implementation and analysis of steady-state Kalman filters with explicit bias compensation;
- Study of the properties of complementary filters;
- Implementation of an advanced solution for integrated roll, pitch and rate gyro bias estimation.

Initially, tests were conducted in the laboratory to gather data on the motion variables measured by the drone's sensors, under different conditions. Next, these were statistically characterised to understand how different physical factors impact the quality of the underlying measurements. Finally, multiple estimation techniques were designed, implemented and analysed, by comparing their results with the values taken as reference - the estimate provided by the quadcopter's built-in estimator.

# 2 Setup and experiments

The experiments conducted, in the laboratory, to gather data to evaluate the various estimation solutions, were the following [2]:

- *Experiment A*: Collecting sensor data with the vehicle at rest, without disturbances from the electric motors - achieved by selecting the "Hover" option for about 30 seconds, without activating the "Take-off" command.
- *Experiment B*: Collecting sensor data with the vehicle on the ground but with the rotors spinning - achieved by selecting the "Hover" option, while applying pressure on the hull (to prevent the vehicle from taking off), and sending the "Take-off" command, waiting for 30 seconds, and, finally, sending the "Land" command.
- *Experiment C*: Collecting sensor data with the vehicle at hover - achieved by selecting the "Hover" option, sending the "Take-off" command, waiting for 30 seconds, and then sending the "Land" command.
- *Experiment D*: Collecting motion sensor data with the vehicle responding to a pitch reference step - achieved by performing the necessary changes in the SIMULINK ARDroneHover.slx model to define a step reference for the pitch angle (as in the experiment conducted for Laboratory 1).
- *Experiment E*: Collecting motion sensor data during a short mission of the UAV - achieved by performing the necessary changes in the SIMULINK ARDroneHover.slx model to define a reference for the  $y$  coordinate, with two waypoints.

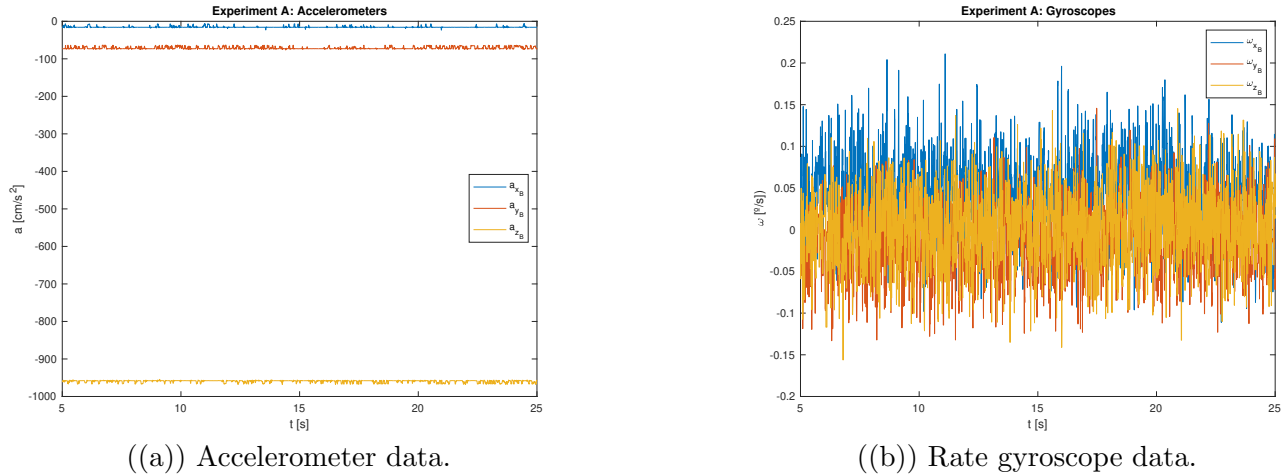
# 3 Modelling and characterisation of the sensors

Knowing the state variables of the quadrotor at each moment, and thus being able to adequately inform the control laws, requires the use of sensors capable of measuring the relevant physical properties for this purpose. However, using real sensors means that these measurements will always be affected by noise and perturbations, which must be studied and quantified in order to design estimators that can minimise the impact of these phenomena on the control of the system.

The experiments described in the previous section were carried out and the data was collected and saved resorting to the Starter Kit provided by the professor. In this section, a statistical analysis of the data collected for experiments *A*, *B* and *C* will be conducted. For these experiments, a period

of approximately 25 s, with the corresponding data, was considered and stored in .mat files which can be read by the SIMULINK files provided in the development kit (using the option *Replay from stored data*) or processed using a MATLAB script.

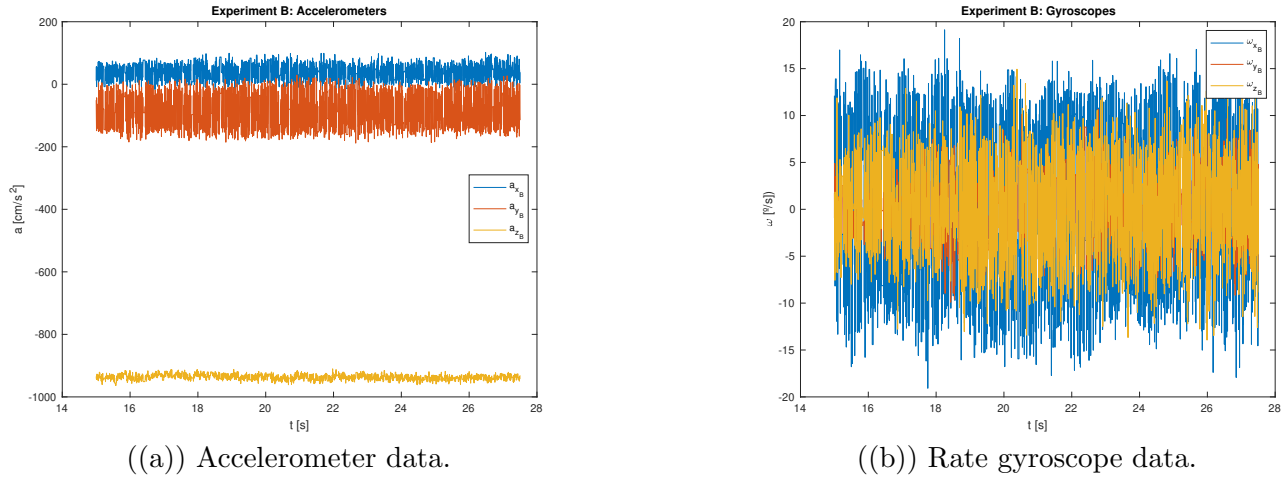
The raw data registered by the accelerometers and gyroscopes for each of the experiments *A* through *C* can be visualised below. Do note that the units of each data signal were left as provided directly by the sensors: the relevant units, inferred by comparing the resulting values with those expected, are, for the accelerometers,  $\text{cm}/\text{s}^2$  and, for the gyroscopes,  $^\circ/\text{s}$ .



((a)) Accelerometer data.

((b)) Rate gyroscope data.

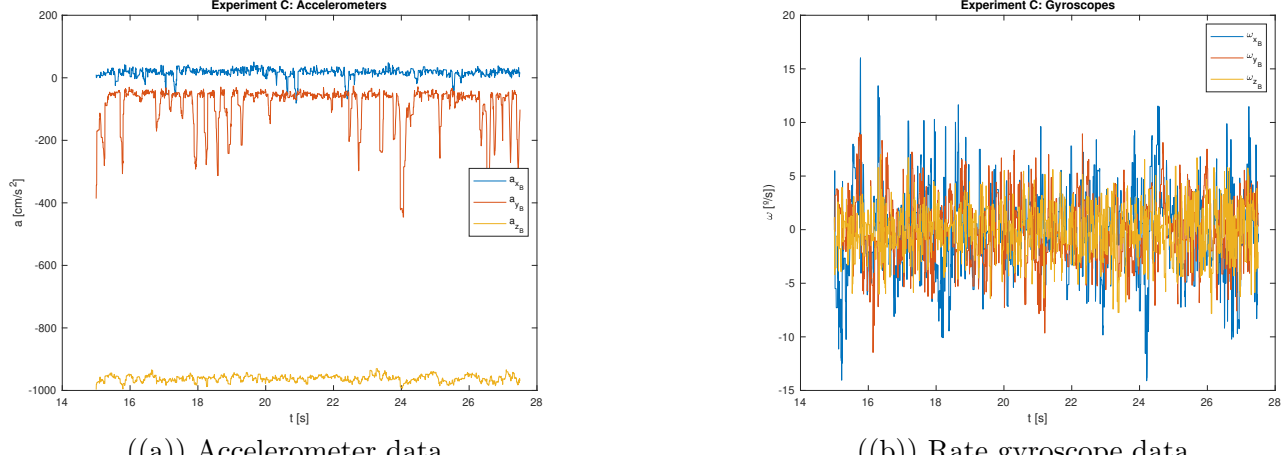
Figure 1: Data gathered for *Experiment A*.



((a)) Accelerometer data.

((b)) Rate gyroscope data.

Figure 2: Data gathered for *Experiment B*.



((a)) Accelerometer data.

((b)) Rate gyroscope data.

Figure 3: Data gathered for *Experiment C*.

### 3.1 Statistical characterisation of the measurements $A$ through $C$

In order to characterise the sensor noise and other disturbances, which can be visualised in figures 1 through 3, the mean and covariance of each of the signals  $a_{x_B}$ ,  $a_{y_B}$ ,  $a_{z_B}$ ,  $\omega_{x_B}$ ,  $\omega_{y_B}$  and  $\omega_{z_B}$  were computed, for each of the three experiments here under analysis. These results are presented in Table 1:

Experiment		$a_{x_B}$ $m[cm/s^2]$	$a_{y_B}$ $m[cm/s^2]$	$a_{z_B}$ $m[cm/s^2]$	$\omega_{x_B}$ $m[deg/s]$	$\omega_{y_B}$ $m[deg/s]$	$\omega_{z_B}$ $m[deg/s]$
		$\sigma^2[cm^2/s^4]$	$\sigma^2[cm^2/s^4]$	$\sigma^2[cm^2/s^4]$	$\sigma^2[deg^2/s^2]$	$\sigma^2[deg^2/s^2]$	$\sigma^2[deg^2/s^2]$
<b>A</b>	<b>mean (<math>m</math>)</b>	-15.44	-71.07	-959.48	0.04201	-0.01344	0.00230
	<b>variance(<math>\sigma^2</math>)</b>	2.987	9.382	8.339	0.00197	0.00156	0.00188
<b>B</b>	<b>mean (<math>m</math>)</b>	37.74	-86.65	-937.09	0.2977	0.3151	0.4692
	<b>variance(<math>\sigma^2</math>)</b>	731.57	3158.4	82.83	84.935	11.154	30.061
<b>C</b>	<b>mean (<math>m</math>)</b>	16.21	-85.82	-961.69	-0.0994	-0.0243	-0.1151
	<b>variance(<math>\sigma^2</math>)</b>	213.73	4790.59	104.28	15.600	8.7023	5.3635

Table 1: Mean and variance for experiments A, B and C.

#### 3.1.1 Experiment A

In this experiment, the quadrotor is resting on the ground, with the rotors off. Thus, it would be expected the measurements be affected by a minimal level of noise, and present a constant bias (if present, at all).

Regarding the accelerometers, one would expect the components of the acceleration along the  $x_B$  and  $y_B$  axes to be null and the component of the acceleration along the  $z_B$  axis to be around  $a_z = -980.66 \text{ cm/s}^2$ . However, note that the mean values of  $a_{x_B}$  and  $a_{y_B}$  are non-null, around  $-15.44 \text{ cm/s}^2$  and  $-71.07 \text{ cm/s}^2$  and the mean of  $a_{z_B}$  is around  $-959.48 \text{ cm/s}^2$ . This suggests that the accelerometer measurements are, in fact, affected by a non-null bias; however, any conclusions taken at this point about the sensor bias are of limited scope, as the disturbances from the motor rotation are not yet present, and the sensors may be calibrated for this condition. Another factor that could be influencing the fact that the accelerations measured along the  $x_B$  and  $y_B$  axes are not the same is the fact that the drone used for all of these tests had one of the four landing struts broken (and held in place by some duct-tape) - this may have resulted in an uneven alignment of the drone, despite being placed on an even surface.

As for the rate gyroscopes, the measurements in all axes were expected to be null. The computed means are, in fact, very close to zero (note that the measurements are expressed in  $^\circ/\text{s}$ ). This suggests that the rate gyros may not be affected at all by bias - however, and for the same reasons expressed for the accelerometers, this consideration requires further analysis.

#### 3.1.2 Experiment B

In this experiment, the quadrotor is actively being held on the ground, with the rotors spinning. Thus, the means of the measurements are expected to be very close to the ones encountered in the previous experiment, and the variances (a good proxy for the level of noise in the signals) to be significantly higher.

This was, in fact, what was found. The most significant difference, in terms of the means, was for the acceleration along the  $x_B$  axis, which was now found to be centred around  $37.74 \text{ cm/s}^2$  (when put into perspective, for example comparing the absolute value of this with the absolute value of the acceleration measured along the  $z_B$  axis, this is not a significant discrepancy). For the rate gyroscopes, compared to *Experiment A*, the mean increased by around one order of magnitude, but is still satisfactorily close to zero. In turn, the variance increase by anywhere between one and three orders of magnitude for the accelerometers, the outlier being the measurement of  $a_{y_B}$ , which suggests the drone is particularly susceptible to disturbances along this axis, and of around four orders of

magnitude for the rate gyros. This experiment also suggests that the accelerometers are affected by a constant bias, while the rate gyros appear to be bias-free.

Nonetheless, it may also be said that the differences between *Experiments A* and *B* weren't only the engine vibrations. The presence of one of the group members holding down the drone was most likely also responsible for some of the errors found. For instance, the drone might have been under too much force, which may have resulted in the deformation of the landing struts, hypothesis which would explain the nonzero accelerometer values. Effects on the variance can also be noted, where the experienced vibrations may have been exacerbated by the effort to keep the drone on the ground.

### 3.1.3 Experiment C

In this experiment, the quadrotor is monitored while hovering at 1m off the ground. Even though this involves having the drone take off and land, the data was segmented so as to consider only the period of time while the vehicle was actually in a steady hover. It is expected that the mean of both the accelerometers and the gyro will be close to that encountered previously and that the variance will be, also, higher than in the first case (*Experiment A*). It would also be unsurprising for the variance to be even higher than the one encountered in *Experiment B* - besides the noise introduced by the spinning rotors (as in the previous dataset), the drone is not kept on a flat surface, instead presenting both some vertical oscillations around the programmed hover height and some sideways drift, quite noticeable while the experiments were being carried out.

Looking at the data, this is not entirely the case. While the means for the accelerometer measurements in this test are consistent with the means found in the previous (which confirms the presence of an at least approximately constant sensor bias, resulting, potentially, from an imperfect installation of the accelerometer on the vehicle body), and the variance for the components of acceleration measured along  $a_{y_B}$  and  $a_{z_B}$  is higher than the one computed for any of the previously analysed cases, a surprising find is that the variance along  $a_{x_B}$  is actually over three times smaller than the one computed for the previous experiment. Comparing the variances found for  $a_{x_B}$  and for  $a_{y_B}$  in this experiment yields a more interesting reflection, suggesting that the drone actually is significantly more immune to drifting, while at a hover, along the  $x_B$ -axis, than along the  $y_B$ -axis (the variance of  $a_{x_B}$  is around 20 times smaller than the variance of  $a_{y_B}$ ).

The statistical characterisation for the the rate gyro is also surprising. The means continue to be close to zero, even if slightly greater than the means computed previously; however, the measured variances are much smaller than the variances computed for *Experiment B* (around one fourth of the variance for  $\omega_{x_B}$  and for  $\omega_{z_B}$ ). Why is the variance increasing, if the drone was subject to, in *Experiment C*, both the noise associated with the motion of the motors and the instability of the hover motion, when compared to an experiment where the drone was being held steady on a fixed surface? These numerical results are easily verified by comparing the figures 2(b) and 3(b): in the former, the graphical representation of  $\omega_{x_B}$  appears as a dense cloud, between  $\pm 15^\circ$ , which is an indication of high frequency variation; in the latter, the representation of the same measurement, while having peaks around the same maximum values ( $\pm 15^\circ$ ), is much more concentrated around the origin and has only occasional peaks of this magnitude, which suggests a lower-frequency variation. The described approach to interpreting this behaviour leads, naturally, to find it logical that the variance in *Experiment B* is higher than the one in *Experiment C*, for the rate gyros. These unexpected findings suggest, once again, that the process of holding the drone down, in the previous experiment, with the rotors spinning, amplified the noise in the sensors' measurements.

Another interesting observation is how the raw acceleration data found in figure 3(a), and in particular the  $a_{y_B}$  component, has almost regularly spaced peaks, corresponding likely to correction manoeuvres performed by the drone's controller to correct the drift along this axis. These peaks appear to be correlated (that is, occurring at the same time) as the peaks in the angular rate  $\omega_{x_B}$  - this would make sense, as the drone is capable of accelerating in the direction of the  $y_B$ -axis only by pitching around the  $x_B$ -axis so as to gain a horizontal acceleration component from the thrust produced by the spinning rotors. Thus, a change in the linear acceleration along the  $y_B$ -axis will

always be accompanied by an angular acceleration around the  $x_B$ -axis.

### 3.2 Using the accelerometers as inclinometers

So far, the accelerometer data has been used as measurements given in the body axes of the vehicle ( $x_B, y_B, z_B$ ). However, the accelerometers are dynamic systems and are not capturing the acceleration of the vehicle itself. Grouping the measurements provided by the three-axis accelerometer as a column vector given by  $\mathbf{a} = [a_x \ a_y \ a_z]^T$ , the relationship between this measured acceleration vector and the acceleration of the quadcopter can be written as

$$\mathbf{a} \propto R^T (\ddot{\mathbf{p}} - g\mathbf{e}_3), \quad (1)$$

where,  $R$  is the rotation matrix from the inertial reference frame to the body reference frame;  $\ddot{\mathbf{p}}$  is the acceleration of the vehicle in the inertial reference frame; and  $\mathbf{e}_3 = [0 \ 0 \ 1]^T$ . Considering that  $\phi$  is the roll angle and  $\theta$  is the pitch angle, and linearising around the equilibrium of the system:

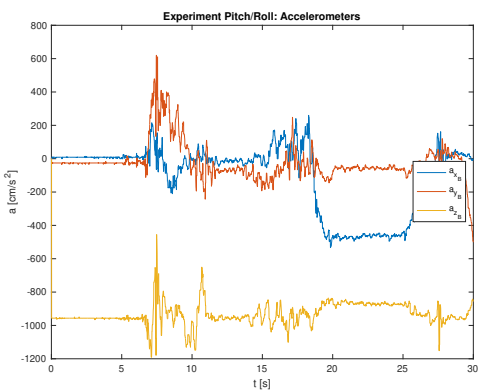
$$\mathbf{a} \propto -g \begin{bmatrix} -\sin \theta \\ \cos \theta \sin \phi \\ \cos \theta \cos \phi \end{bmatrix}. \quad (2)$$

From the relationship between the vectors expressed in 2, it is possible to easily obtain expressions for the estimates of the roll ( $\phi$ ) and pitch ( $\theta$ ) angles, which will be from here on referred to as "raw".

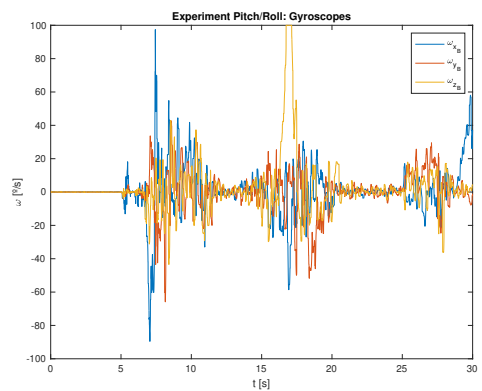
$$\phi = \arctan \frac{a_y}{a_z}, \quad \theta = \arctan \frac{a_x}{\sqrt{a_y^2 + a_z^2}} \quad (3)$$

In this manner, it is relatively easy to convert the accelerometer measurements into raw angle estimates. The results of this rudimentary calculation may be compared to the better estimate, taken as a reference, provided by the quadcopter's built-in controller/estimator. The two signals just mentioned are labelled, in the graphs present in figure 5, respectively, as "raw inclinometer" and "real (euler)".

For this purpose, a separate experiment was carried out, which will be designated as *Experiment Pitch/Roll*. Here, sensor data was collected with the drone switched on, with the electric motors off, while being manipulated by a member of the group. In this manner, it was possible to gather data with the drone at relatively extreme roll and pitch angles (as much as  $20^\circ$  to  $30^\circ$ ). Note that this data is not affected by disturbances from the electric motors (less high-frequency noise is expected); however, there is always a degree of uncertainty arising from the fact that all deflections were carried out "manually", with no precise references or stabilisation mechanisms. The raw accelerometer and gyroscope data gathered from the execution of this experiment can be visualised in figure 4 - as can be seen, the experiment begins with the quadcopter being held approximamately level; around the 7-second mark, the drone was set in a position corresponding to a roll angle of approximately  $-20^\circ$ ; around the 20-second mark, the drone is set in a position corresponding to a pitch angle of approximately  $-30^\circ$ .

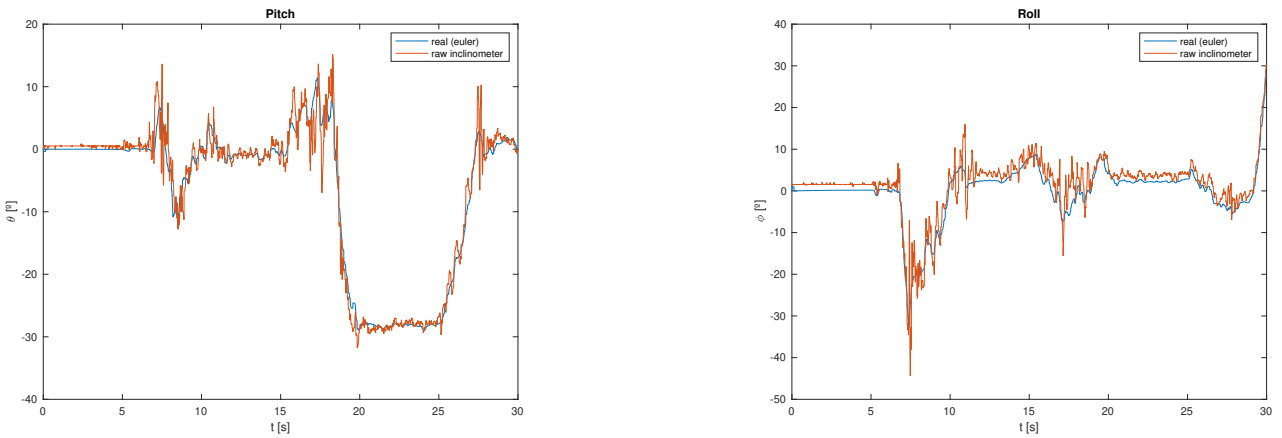


((a)) Accelerometers data.



((b)) Rate gyroscopes data.

Figure 4: Raw data gathered for *Experiment Pitch/Roll*.



(a)) Pitch: raw computation and reference.

(b)) Roll: raw computation and reference.

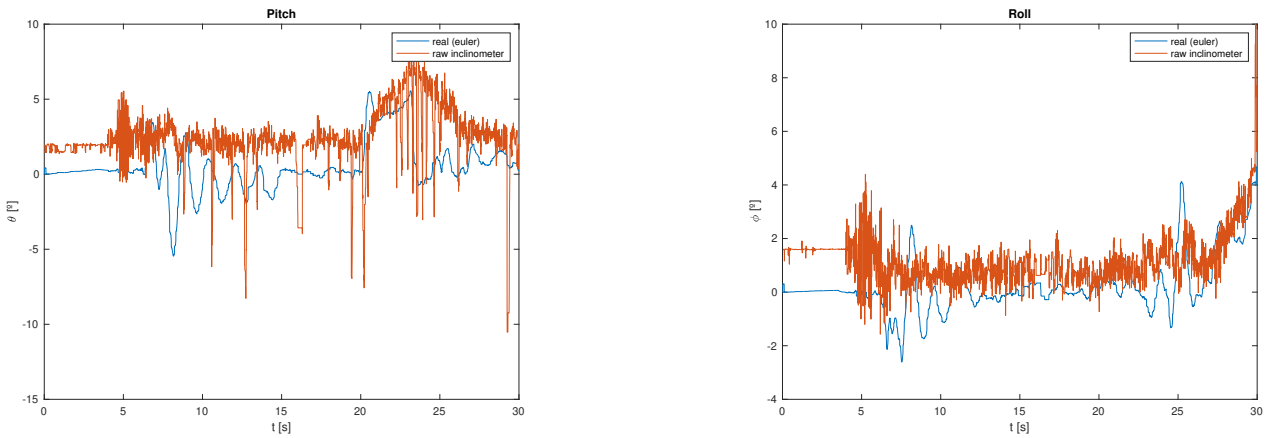
Figure 5: Comparison of the pitch ( $\theta$ ) and roll ( $\phi$ ) angles computed using the above-described approximation ("raw inclinometer") with the measurements provided by the quadcopter's integrated estimator ("real (euler)"), for *Experiment Pitch/Roll*.

From the graphs of figure 5, it is visible that the "raw" angle measurements are relatively close to the ones provided by the integrated estimator, taken as the "real" reference values. Particularly visible in the second graph (for the roll angle) is what appears to be a small but relatively constant offset. However, what distinguishes the two measurements the most is the smoothness of the reference values, when compared to the "raw" ones: the latter values appear to be a lot more volatile, presenting, on multiple occasions, peaks corresponding to large deviations from the reference.

In general, the results obtained from using the accelerometers directly as an inclinometer are consistent with the more sophisticated estimator employed by the drone's onboard computer, which leads us to consider this approach to be moderately successful. Using this "raw" data for a feedback controller would likely not yield good results, as it would result in an over-actuation of the controller as a response to the noise-induced peaks that can be visualised; however, this method for estimating the euler angles of the drone could have some potential, if further smoothing of the data is possible.

Note, as well, that the way this experiment was carried out may have impacted the results obtained. As the electric motors were switched off for this experiment, the lack of disturbances originating from their rotation means that the results may not be representative of the ones to be found during normal operation of the drone. Moreover, the angles here used are larger than the ones that are expected to be found during nominal operation, and there is no clear reason to assume the results would be as good with smaller angular deflections. For this reason, the same script for comparing the raw inclinometer data with the estimation provided by the quadcopter was run but using the results from *Experiment D*. The results can be visualised in figure 6: the drone was configured to follow a 0.15 rad (around 8.6°) step in the pitch reference, lasting 3 s, given 20 s into the experiment.

In these graphs, the limitations of this method of estimation are a lot clearer. There is an offset of around 2° between the angle estimates, both for the pitch and roll measurements; and the non-smoothness of the data originating from the "raw" computation is even clearer, given the increased detail of the vertical scale of the graphs here. This offset can be partially explained by the fact that the accelerometer is not mounted perfectly flat on the drone body. The drone estimator can account for this fact, but the raw calculations cannot. A possible solution around this problem could be calibrating the accelerometer measurements in the  $x_B$  and  $y_B$  axis to 0 and the  $z_B$  acceleration to  $-9.81 \text{ m/s}^2$  in the beginning of the experiment. This method was used in the data in section 5.



((a)) Pitch: raw computation and reference.

((b)) Roll: raw computation and reference.

Figure 6: Comparison of the pitch ( $\theta$ ) and roll ( $\phi$ ) angles computed using the above-described approximation ("raw inclinometer") with the measurements provided by the quadcopter's integrated estimator ("real (euler)"), for *Experiment D*.

## 4 Kalman Filters

In this section, a simplified Kalman filter for estimating the pitch and roll angles of the quadrotor was designed and implemented. A possible representation for this type of filters can be obtained from the state space model, explicitly considering the observation noise ( $\mathbf{v}$ ) and the process noise ( $\mathbf{w}$ ), as shown below: [3]

$$\begin{aligned} \dot{\mathbf{x}} &= A\mathbf{x} + B\mathbf{u} + G\mathbf{w}. \\ \mathbf{y} &= C\mathbf{x} + D\mathbf{u} + H\mathbf{w} + \mathbf{v} \end{aligned} \quad (4)$$

Considering the noises  $\mathbf{v}$  and  $\mathbf{w}$  to be white, uncorrelated noise (that is, considering that the equalities  $E[\mathbf{w}] = E[\mathbf{v}] = 0$ ,  $E[\mathbf{w}\mathbf{w}^T] = Q$ ,  $E[\mathbf{v}\mathbf{v}^T] = R$ , and  $E[\mathbf{w}\mathbf{v}^T] = 0$  hold), the following solution follows:

$$\dot{\hat{\mathbf{x}}} = A\hat{\mathbf{x}} + B\mathbf{u} + L(\mathbf{y} - C\hat{\mathbf{x}} - D\mathbf{u}), \quad (5)$$

where  $\hat{\mathbf{x}}$  is the vector corresponding to the estimated state,  $\mathbf{u}$  is the system input,  $\mathbf{y}$  the output and  $L = PCTR^{-1}$  is the Kalman gain, with  $P$  being the error covariance matrix:

Considering the system to be continuous, linear and time invariant, yields the following relationship between matrix  $P$  and the more commonly used matrixes  $Q$  and  $R$ :

$$AP + PA^T + Q - PC^TR^{-1}CP = 0 \quad (6)$$

### 4.1 Kalman filter for pitch/roll estimation: design & implementation

Linearizing the kinematics of the rotational movement (described in equation 7) as was done in the previous laboratory work, one obtains the following result:  $\begin{bmatrix} \dot{\phi} \\ \dot{\theta} \end{bmatrix} = \begin{bmatrix} p \\ q \end{bmatrix}$ .

$$\begin{bmatrix} \dot{\phi} \\ \dot{\theta} \\ \dot{\psi} \end{bmatrix} = \begin{bmatrix} 1 & \sin \phi \tan \theta & \cos \phi \tan \theta \\ 0 & \cos \phi & -\sin \phi \\ 0 & \frac{\sin \phi}{\cos \theta} & \frac{\cos \phi}{\cos \theta} \end{bmatrix} \begin{bmatrix} p \\ q \\ r \end{bmatrix} \quad (7)$$

#### 4.1.1 Pitch

Considering that the value measured by the rate gyro, relative to the  $y_B$ -axis, is given by the sum of the value of the pitch angular velocity with the process noise, that is,  $\omega_{ym} = \dot{\theta} + n_\theta$  and taking the gyro measurements as the system input and the pitch angle provided by the inclinometer as the output, the values for the A, B, C and D matrixes, for the pitch estimation, are:

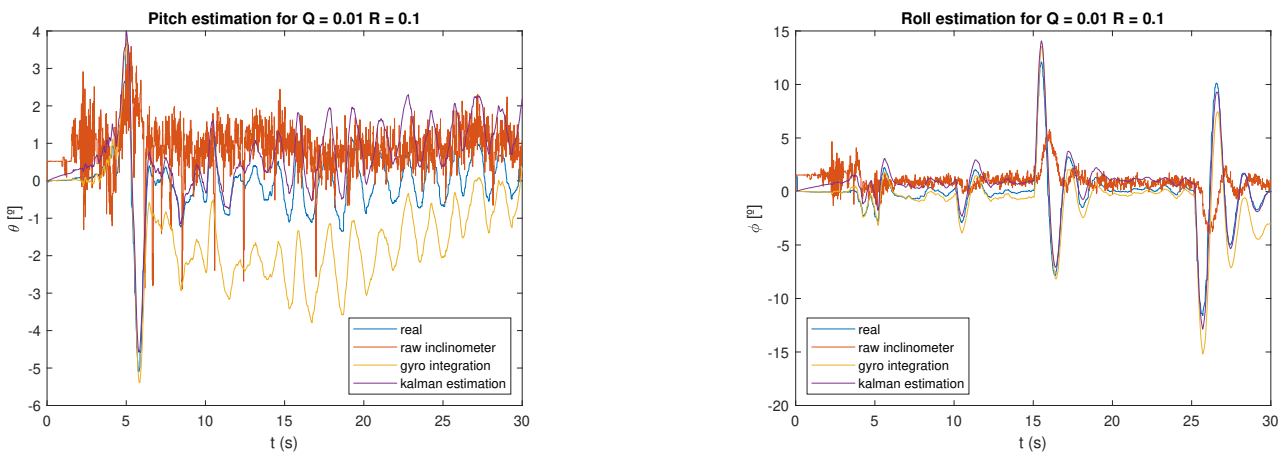
$$A = 0, B = 1, C = 1, \text{ and } D = 0.$$

Thus, the evolution of the pitch angle estimate will be guided by the integration of the gyroscope measurements, and corrected by the inclinometer output. To use the MATLAB-provided `kalman()`

function, it is still necessary to define the values of  $Q$ ,  $R$ , as well as  $G = 1$  and  $H = 0$ , from the assumptions described above. The ultimate values settled on for  $Q$  and  $R$  were, after an iterative analysis,  $Q = 10^{-2}$  and  $R = 10^{-1}$ . This method works, globally, because the system is observable (the observability matrix,  $\mathcal{O} = C = 1$ , has a rank equal to the number of states considered in the model).

Having generated the state space model corresponding to this estimator, as well as the Kalman gain, the next step is loading the results for *Experiment E*, and comparing with the attitude measurements provided by the drone's built-in estimator (labelled as "real"), with the raw inclinometer data obtained in 3.2 (labelled as "raw inclinometer"), the data obtained by purely integrating the gyroscope measurements (labelled as "gyro integration") and the results provided by the Kalman filter just described. These can be seen in figure 7(a).

As can be seen, the estimation provided by the Kalman filter is better than the ones found so far (raw accelerometer calculation); however, it seems to be drifting away from the drone's estimation. This behaviour may be a result of bias in the estimation (on the one hand, as  $R > Q$ , more importance is being attributed to the gyroscope in the estimation process, for which no explicit compensation method is currently being used; on the other hand, the accelerometer bias visible in the raw data [3] is affecting the inclinometer data, which also affects the quality of this). In any way, the result of this estimation process is much better than the raw data provided by the inclinometer measurement (which is subject to a great deal of noise and has limited capacity to follow larger angular deflections, a result of its low data rate) and is also better than purely integrating the gyroscopes - this approach is subject to an even greater level of drift. This method could be improved by explicitly subtracting the bias measured in the accelerometer data, as described in the end of section 3.2.



((a)) Pitch: raw computation and reference.

((b)) Roll: raw computation and reference.

Figure 7: Comparison of pitch and roll angle estimates from raw accelerometer data, from the integration of the rate gyro and from the Kalman filter with the reference values.

#### 4.1.2 Roll

An analogous approach can be done for the estimation of the roll angle, in this case, considering  $\omega_{xm} = p + n_\phi$ . This means that the value measured by the rate gyroscope around the  $x_B$ -axis is the sum of the angular roll rate with the process noise. Using the simplified expression derived from the linearization of 7, the state space model obtained is equivalent to the one described above, still using as system input the gyroscope measurement, but now taking as the system output the roll angle given by the inclinometer. For the sake of comparison, the same initial values as before were considered for  $Q$  and  $R$  ( $Q = 10^{-2}$  and  $R = 10^{-1}$ ). The same process as the one described above was carried out for obtaining the model for this estimator, and the evaluation of the results thus provided was done in the same way (comparing the different estimation methods for the data gathered in *Experiment E*). These results can be seen in figure 7(b).

The estimation provided by the Kalman filter appears to be consistent with the quality of the one obtained for the pitch. Some drift between the reference measurements and the Kalman-provided estimate is still visible, particularly in sections where the roll angle is approximately constant (likely another consequence of the imperfect installation of the accelerometer). Curiously, the Kalman estimate and the reference values (drone's internal estimate) tend to converge in the vicinity of peaks (note the peaks visible around 15 s and around 25 s). In these peaks, as greater importance is being given to the gyroscope measurements, which have a greater capacity to track large angular deflections, when compared to the inclinometer data, the Kalman estimate is able to accompany these satisfactorily.

## 4.2 Transfer function

From the equation for the solution of the state estimates (equation 5), it is possible to write  $\dot{\mathbf{x}} = A'\mathbf{x} + B'\mathbf{u}'$ , where  $\mathbf{u}' = \begin{bmatrix} \mathbf{u} \\ \mathbf{y} \end{bmatrix}$ ,  $A' = A - LC$ ,  $B' = [B \ L]$ . To obtain the theoretical transfer functions, simply apply the Laplace transform with null initial conditions, and then compute the transfer functions using the relevant variable in each case (separately, for the pitch and roll estimation).

$$X(s) = (sI - A')^{-1} B' U'(s) \quad (8)$$

### 4.2.1 Pitch

Taking  $x = \hat{\theta}$  and  $\mathbf{u}' = [w_{ym} \ \theta_m]^T$ , the transfer function for the Kalman filter estimate of the pitch angle, represented as  $\hat{\theta}_m$ , relative to the pitch angle indicated by the inclinometer,  $\theta_m$ , is:

$$\frac{\hat{\Theta}(s)}{\Theta_m(s)} = \frac{L}{s + L} = \frac{0.3162}{s + 0.3162}, \quad (9)$$

In turn, the transfer function from the rate gyro measurement,  $\omega_m$ , to the Kalman pitch estimate,  $\hat{\theta}_m$ , is

$$\frac{\hat{\Theta}(s)}{\Omega_{ym}(s)} = \frac{1}{s + L} = \frac{1}{s + 0.3162} \quad (10)$$

Note that substituting L for a numeric value was achieved by using the  $Q$  and  $R$  values above considered and computing the Kalman gain with MATLAB.

These transfer functions correspond to first-order low-pass filters. Note as well that, while 9 has unitary gain (this means that the value of  $L$  does not change the static gain of the transfer function), the static gain of 10 tends to diminish with the increase of the Kalman gain,  $L$  (this corresponds to making the estimate more dependent on the inclinometer data).

### 4.2.2 Roll

Taking  $x = \hat{\phi}$  and  $\mathbf{u}' = [w_{xm} \ \phi]^T$ , and using the same values for  $Q$  and  $R$  (since the sensors are the same), the transfer function for the Kalman filter estimate of the roll angle, represented as  $\hat{\phi}_m$ , relative to the roll angle indicated by the inclinometer,  $\phi_m$ , is:

$$\frac{\hat{\Phi}(s)}{\Phi(s)} = \frac{L}{s + L} = \frac{0.3162}{s + 0.3162} \quad (11)$$

And, finally, the transfer function from the rate gyro measurement,  $\omega_m$ , to the Kalman pitch estimate,  $\hat{\theta}_m$ , is

$$\frac{\hat{\Phi}(s)}{\Omega_{xm}(s)} = \frac{1}{s + L} = \frac{1}{s + 0.3162} \quad (12)$$

The behaviour of these transfer functions is the same as described in the case of the pitch.

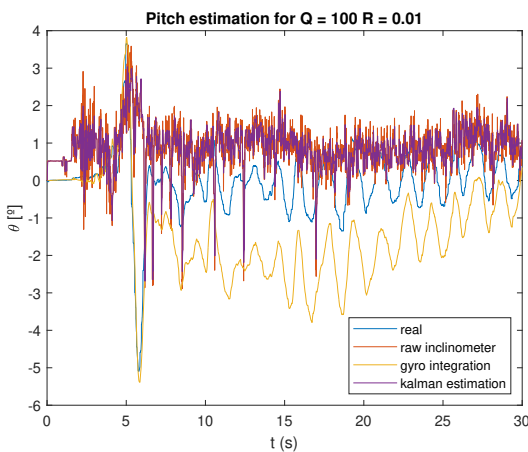
### 4.3 Parameters Q and R

The  $Q$  and  $R$  matrices can be interpreted as covariance matrices, associated, respectively, with the rate gyroscope and with the inclinometer measurements. In this model, the matrices are scalars, and so a higher value of  $Q$  or  $R$  translates directly to the covariance of the measurement at hand, i.e., the uncertainty associated with that measurement, is greater. The estimator will tend to "ignore" more the sensor/model with a higher covariance, and follow more closely the measurements provided by the more accurate sensor/model. Thus, increasing  $Q$  means that the estimator will follow the inclinometer more closely, and increasing  $R$  means that the estimator output will be more based on the gyroscope.

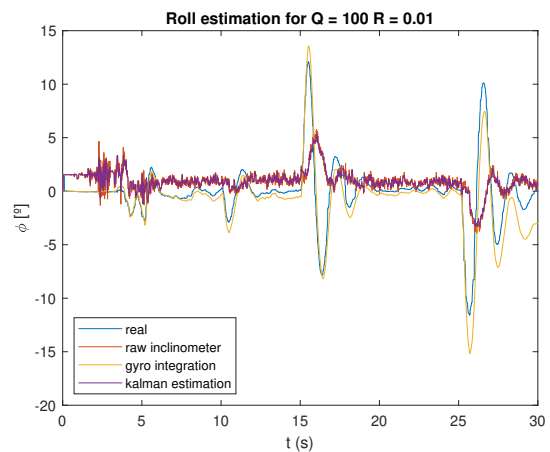
The impact on the Kalman gain  $L$  can easily be computed as well, recovering equations 6 and the relationships  $\mathbf{L} = \mathbf{P}\mathbf{C}^T\mathbf{R}^{-1}$  and  $\mathbf{Q} - \mathbf{P}\mathbf{R}^{-1}\mathbf{P} = 0$  (a consequence of  $Q$  and  $R$  are scalar). Combining these to write  $L$  as a function of  $P$  yields:

$$L = \sqrt{\frac{Q}{R}} \quad (13)$$

Interpreting the impact of parameters  $Q$  and  $R$  from the perspective of their impact on the Kalman gain leads us to conclude that increasing  $Q$  ("mistrusting" the gyroscope) leads to an increase of  $L$ . Inversely, increasing  $R$  ("mistrusting" the inclinometer) leads to a decrease of  $L$ . The following figures represent this behaviour.



((a)) Pitch: raw computation and reference.

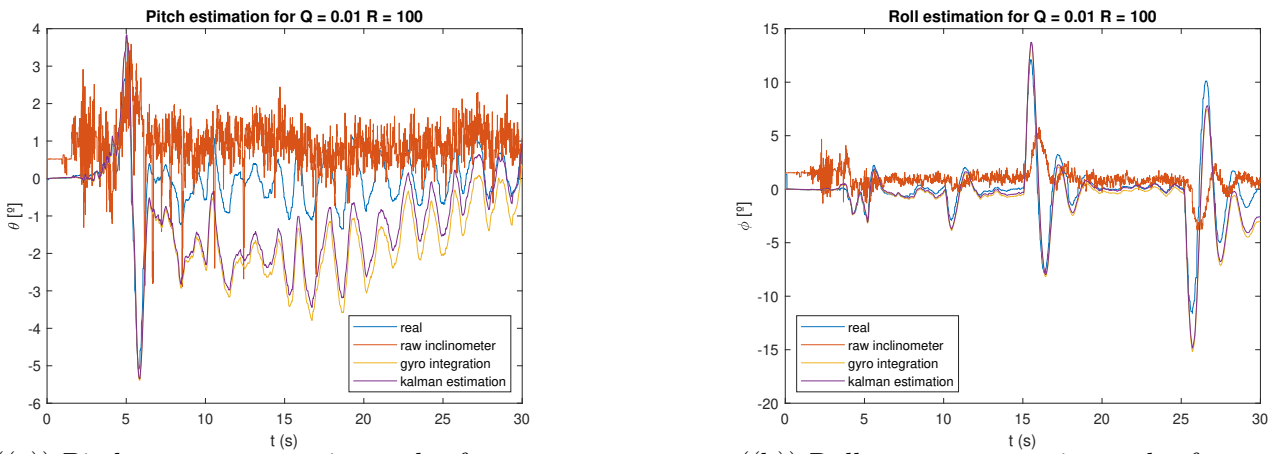


((b)) Roll: raw computation and reference.

Figure 8: Comparison of pitch and roll angle estimates from raw accelerometer data, from the integration of the rate gyro and from the Kalman filter with the reference values, for different values of  $Q$  and  $R$  ( $Q \gg R$ ).

In figures 8(a) and 8(b), the response of the filter for the pitch and roll angles, respectively, can be seen, using a much higher value for  $Q$  than for  $R$ . This choice of parameters corresponds to, as seen above, a high Kalman gain  $L$ , which means essentially ignoring the gyroscope and placing a lot of trust in the inclinometer data. This behaviour is easy to observe: in both cases, the Kalman estimate closely tracks the raw inclinometer measurements (albeit with some attenuation of the peaks).

As for figures 9(a) and 9(b), these represent the response of the filter for the pitch and roll angles, respectively, using a much lower value for  $Q$  than for  $R$ . This provides a low Kalman gain  $L$ , which means more trust will be given to the gyroscope data. Again, this behaviour is easy to observe: in both cases, the Kalman estimate is now closely tracking the measurements obtained from direct integration of the angular velocities registered by the rate gyro.



((a)) Pitch: raw computation and reference.

((b)) Roll: raw computation and reference.

Figure 9: Comparison of pitch and roll angle estimates from raw accelerometer data, from the integration of the rate gyro and from the Kalman filter with the reference values, for different values of  $Q$  and  $R$  ( $R \gg Q$ ).

#### 4.4 Including gyro bias as an extra state

In this stage, a new Kalman filter is developed, this time considering two states: as well as the measurement to be estimated, including the bias associated with that measurement as a separate state. For this effect, the bias is considered to be constant (time-invariant), this is, represented as  $b_y$  or  $b_x$  such that  $\dot{b}_y = \dot{b}_x = 0$ . This seems to be a valid approximation, taking into account the conclusions of section 3.2. Thus, one can rewrite both  $\omega_{ym}$  and  $\omega_{xm}$  as  $\omega_{ym} = q + b_y + n_\theta$  and  $\omega_{xm} = p + b_x + n_\phi$ , respectively.

Via the same process described in 4.1, the state-space model may be defined,

$$A = \begin{bmatrix} 0 & -1 \\ 0 & 0 \end{bmatrix}, \quad B = \begin{bmatrix} 1 \\ 0 \end{bmatrix}, \quad C = [1 \ 0], \quad D = 0, \quad (14)$$

and its observability may be computed,  $\mathcal{O} = \begin{bmatrix} C \\ CA \end{bmatrix} = \begin{bmatrix} 1 & 0 \\ 0 & -1 \end{bmatrix}$ . As the matrix has maximum rank, the system is observable.

Assuming values for G, H, Q and R:

$$G = \begin{bmatrix} 1 & 0 \\ 0 & 1 \end{bmatrix}, \quad H = [0 \ 0], \quad Q = \begin{bmatrix} 8 \times 10^{-3} & 0 \\ 0 & 1.5 \times 10^{-3} \end{bmatrix}, \quad R = 1 \times 10^{-2},$$

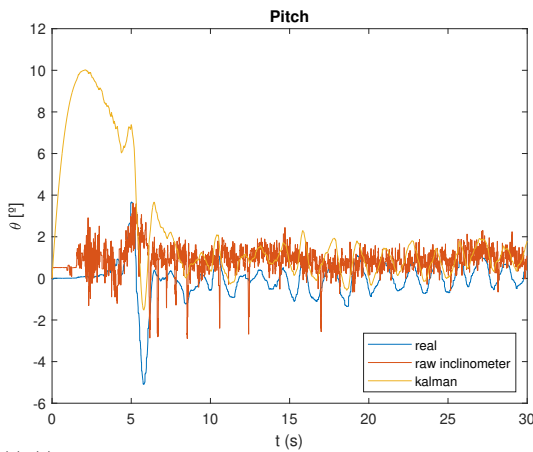
one may now obtain the estimator state-space model.

The effectiveness of this model was validated by artificially introducing a bias of  $+6^\circ/\text{s}$  in the roll rate gyro measurements and of  $+12^\circ/\text{s}$  in the pitch rate gyro measurements and running this data through the newly obtained filter. This approach yielded very satisfactory results (note in figure 11(b) how the estimated bias tends to the artificially introduced bias, in each case). In figures 10(a) and 10(b), the overall response of the filter can be compared with the reference values, as well as with the raw inclinometer data. The catastrophic results that would be obtained from simply integrating the gyroscope measurements (affected by the bias) can be seen in figure 11(a) and tend, as expected, to a straight line with a slope close to the bias introduced.

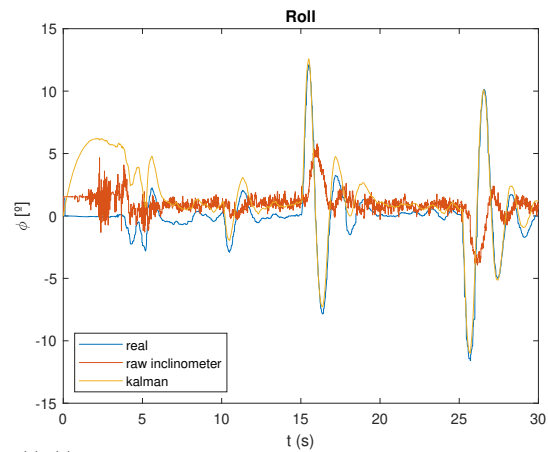
#### 4.5 Complementary filters

Complementary filters are filters that, when used jointly, have the capacity to cover the whole range of frequencies occurring in the system. Usually, these are the sum of a low-pass filter with a high-pass filter. For two filters to be complementary, the sum of their transfer functions must be unitary, this is, considering a filter  $H_1(s)$  and a filter  $H_2(s)$ ,  $H_1(s) + H_2(s) = 1$ .

This class of filter does not require the inclusion of the system input in the kinematic model, or even the modelling of the system dynamics, so it is easy to implement. It is only necessary to study

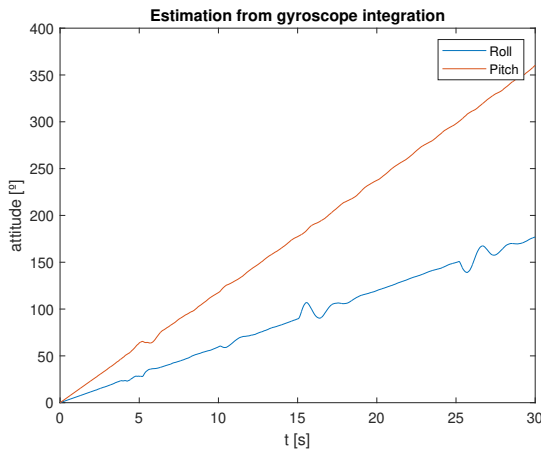


((a)) Pitch: raw computation and reference.

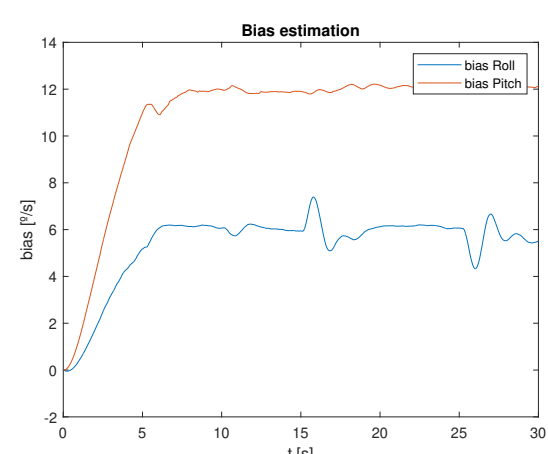


((b)) Roll: raw computation and reference.

Figure 10: Comparison of pitch and roll angle estimates from raw accelerometer data, and from the state-expanded Kalman filter with the reference values, with an artificial bias in the gyro data.



((a)) Attitude resulting from biased gyroscope integration.



((b)) Bias estimated by the kalman filter.

Figure 11: Pitch and roll estimates that would be obtained by integrating the biased gyro data, and biases estimated by the filter - note how these estimates converge, in fact, to the introduced values of  $+6^\circ/\text{s}$  (roll) and of  $+12^\circ/\text{s}$  (pitch).

the vehicle sensors and designing the estimator from the observer model; in this manner, dynamics or phenomena that were not modelled will not affect the quality of the resulting estimates. On the one hand, this can be an advantage, as it makes this type of filters easier to implement; on the other hand, not taking into account the dynamics of the system is limiting.

The estimation of the pitch angles, as computed over the course of this laboratory session, are a combination of the inclinometer measurements (filtered by a low-pass filter) and the integration of the rate gyro measurements (filtered by a high-pass filter). The same holds true for the roll angle estimates, so only the case of the pitch will be analysed in detail.

#### 4.5.1 Without including gyro bias as extra state

From the transfer functions obtained for the pitch angle, described in detail in section 4.2, one can compute the result obtained by summing them. Note that the division by  $s$  in the first term of the sum represents the integration carried out for the rate gyro data.

$$\frac{\hat{\Theta}(s)}{\Omega_{ym}(s)/s} + \frac{\hat{\Theta}(s)}{\Theta_{inc}(s)} = \frac{s}{s+L} + \frac{L}{s+L} = 1, \quad (15)$$

Independently from the Kalman gain  $L$  used, the sum of both transfer functions will always be

1. This corroborates the hypothesis that these filters for the inclinometer and for the gyroscope are complementary.

Another way of reaching this conclusion would be recalling, as mentioned before, that the gyroscope measurements are affected by low-frequency noise, while the inclinometer measurements are affected by high-frequency noise. Thus, filtering both measurements effectively would require employing a high-pass filter (in the first case) and a low-pass filter (in the second case). Thus, they would complement each other; ensuring the sum is normalised would be the last requirement.

#### 4.5.2 Including gyro bias as extra states

The same analysis can be carried out for the case where the bias is also considered as a state in the model. Recalling the relationships  $\begin{bmatrix} \dot{\phi} \\ \dot{\theta} \end{bmatrix} = \begin{bmatrix} p \\ q \end{bmatrix}$  and  $\omega_{ym} = q + b_y + n_\theta$ , the sum of the two relevant transfer functions (decomposing the Kalman gain into its two components  $l_1$  and  $l_2$ ), yields equation 16, from which it is concluded that the filters are complementary.

$$\frac{\hat{\Theta}(s)}{\Omega_{ym}(s)/s} + \frac{\hat{\Theta}(s)}{\Theta_{inc}(s)} = \frac{s^2}{s^2 + l_1 s + l_2} + \frac{l_1 s + l_2}{s^2 + l_1 s + l_2} = 1. \quad (16)$$

### 4.6 Discussion of the results obtained

In table 2, the root mean square error for the attitude estimates using 4 different methods and for 6 different tests is presented.

RMS (deg)	Experiments												Mean RMS	
	A		B		C		D		E		Pitch/roll test			
	Pitch	Roll	Pitch	Roll	Pitch	Roll	Pitch	Roll	Pitch	Roll	Pitch	Roll	Pitch	Roll
Raw inclinometer	0.352	2.252	1.140	5.471	1.534	5.319	2.931	1.380	1.421	3.138	2.102	2.749	1.580	3.385
Gyroscope integration	0.570	0.267	0.944	0.887	2.670	1.894	2.473	1.069	1.593	1.274	1.893	3.492	1.690	1.480
Kalman filter (without bias estimation)	0.359	2.093	0.734	4.513	1.391	3.578	1.790	0.946	0.824	0.946	1.306	2.802	1.068	2.479
Kalman filter (with bias estimation)	0.306	2.265	0.788	5.126	0.855	4.299	2.129	1.108	0.978	1.129	1.085	2.304	1.023	2.705

Table 2: Comparison of the performance of the different methods in estimating the attitude. The RMS was calculated for several methods and for several tests, taking as a reference the estimate provided by the drone's built-in estimator.

As was expected, the RMS values of experiment A are lower than those of experiment B, since the motors are turned on in this second experiment. It is inferred that the vibration negatively impacts the performance of the Kalman filter, as well as that of the other methods, in some cases doubling the RMS value.

Also looking at the mean RMS for each method, it can be noticed that the accuracy of the estimations is better for the Kalman filter than for the raw inclinometer data. The gyroscope integration method, at first glance, seems to provide good results, but that is only true for experiments where the drone was fixed to the ground (experiments A and B). These low values of RMS, in turn, lower the mean RMS for this method that appears in the final column. Therefore, this value does not translate accurately the efficacy of this method.

## 5 Integrated roll and pitch estimation

For the final section of this laboratory, the solution presented in Batista *et al.* [1] was studied and implemented. It is known that it is impossible to recover the attitude with a single vector observation (indeed, one degree of freedom is unobservable); however, this approach allows for partial attitude reconstruction as well as estimation of rate gyro biases through a single vector observation.

## 5.1 Observability

The system dynamics are given by

$$\begin{cases} \dot{\mathbf{x}}(t) = \mathbf{A}(\mathbf{y}(t), \boldsymbol{\omega}_m(t))\mathbf{x}(t) + \mathbf{B}\mathbf{u} \\ \mathbf{y}(t) = \mathbf{C}\mathbf{x}(t) + \mathbf{D}\mathbf{u} \end{cases} \quad (17)$$

where  $\mathbf{x} = [\mathbf{x}_1^T \quad \mathbf{x}_2^T]^T$  is the state vector,  $\mathbf{y}$  is the system output,  $\boldsymbol{\omega}_m = \boldsymbol{\omega} + \mathbf{b}_\omega$  are the rate gyro measurements corrupted with bias,  $\mathbf{B} = 0 \in \mathbb{R}^{6 \times 1}$ ,  $\mathbf{D} = 0$  and

$$\mathbf{x}_1 = \begin{bmatrix} y_{a_x} \\ y_{a_y} \\ y_{a_z} \end{bmatrix}, \quad \mathbf{x}_2 = \begin{bmatrix} b_{\omega_x} \\ b_{\omega_y} \\ b_{\omega_z} \end{bmatrix}, \quad \mathbf{A} = \begin{bmatrix} -\mathbf{S}(\boldsymbol{\omega}_m(t)) & -\mathbf{S}(\mathbf{y}(t)) \\ 0_{3 \times 3} & 0_{3 \times 3} \end{bmatrix} \in \mathbb{R}^{6 \times 6}, \quad \mathbf{C} = [I_{3 \times 3} \quad 0_{3 \times 3}] \in \mathbb{R}^{3 \times 6} \quad (18)$$

with  $\mathbf{S}$  the skew-symmetric operator such that  $\mathbf{S}(\mathbf{x})\mathbf{y} = \mathbf{x} \times \mathbf{y}$ .

Though the system described in 18 is nonlinear, it can be thought of as a linear time-varying system. Though the progression of the system resembles the response of a linear system, it is not given by the superposition of the free and forced responses. Nonetheless, this is irrelevant for the purposes of observability since the input and output are available. According to theorem 3.4 of [1], the pair  $(\mathbf{A}(t), \mathbf{C})$  is uniformly observable.

## 5.2 Kalman filter design

Considering now additive system disturbances and sensor noise, it is possible to write the dynamics as

$$\begin{cases} \dot{\mathbf{x}}(t) = \mathbf{A}(\mathbf{y}(t), \boldsymbol{\omega}_m(t))\mathbf{x}(t) + \mathbf{w}(t) \\ \mathbf{y}(t) = \mathbf{C}\mathbf{x}(t) + \mathbf{n}(t) \end{cases} \quad (19)$$

where  $\mathbf{w}(t) \in \mathbb{R}^6$  and  $\mathbf{n}(t) \in \mathbb{R}^3$  are uncorrelated zero-mean white Gaussian noise and  $E[\mathbf{w}(t)\mathbf{w}^T(t)] = Q \succ 0$ ,  $E[\mathbf{n}(t)\mathbf{n}^T(t)] = R \succ 0$ .

The covariance matrix propagation is given by

$$\dot{\mathbf{P}}(t) = \mathbf{A}(t)\mathbf{P}(t) + \mathbf{P}(t)\mathbf{A}^T(t) + \mathbf{Q} - \mathbf{P}(t)\mathbf{C}^T\mathbf{R}^{-1}\mathbf{C}\mathbf{P}(t) \quad (20)$$

Then, the Kalman gain is given by equation 21.

$$\mathbf{K}(t) = \mathbf{P}(t)\mathbf{C}^T\mathbf{R}^{-1} \quad (21)$$

Finally, with the computed Kalman gain  $\mathbf{K}(t)$ , the Kalman filter equations are

$$\hat{\mathbf{x}}(t) = \mathbf{A}(t)\hat{\mathbf{x}}(t) + \mathbf{K}(t)[\mathbf{y}(t) - \mathbf{C}\hat{\mathbf{x}}(t)] \quad (22)$$

Figure 12 depicts the Simulink block diagram of the implemented system.

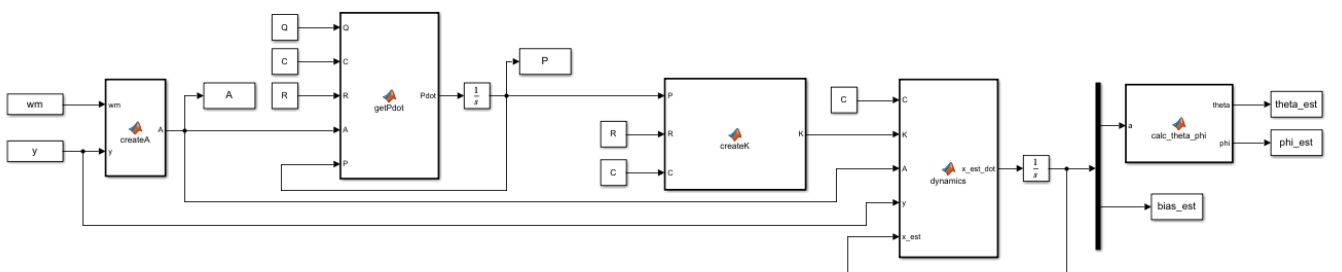
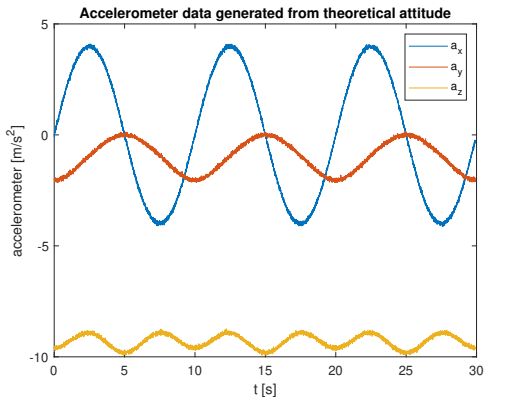


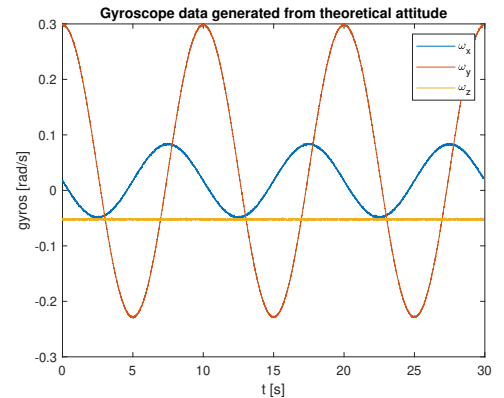
Figure 12: Block diagram of the implemented Kalman filter.

### 5.3 Validation

In order to validate the Kalman filter, the simulation described in [1] was also performed. As such, the roll and pitch angle inputs were sinusoidal waves. Bias was considered in the rate gyro measurements, set to  $[1 \ 2 \ -3]^T \frac{\pi}{180}$  rad/s, as well as sensor noise modelled as additive zero-mean Gaussian noise with standard deviation of  $0.05 \text{ m s}^{-2}$  for the accelerometer measurements and  $0.05 \frac{\pi}{180}$  rad/s for the rate gyro measurements.



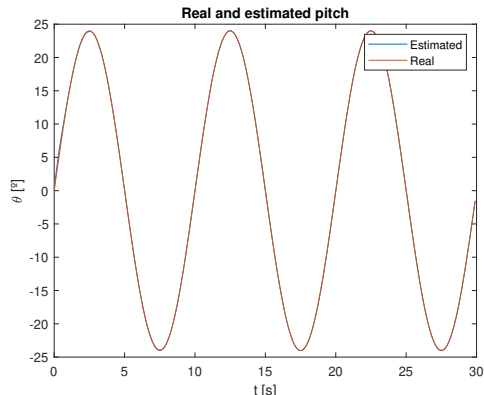
((a)) Accelerometer theoretical data.



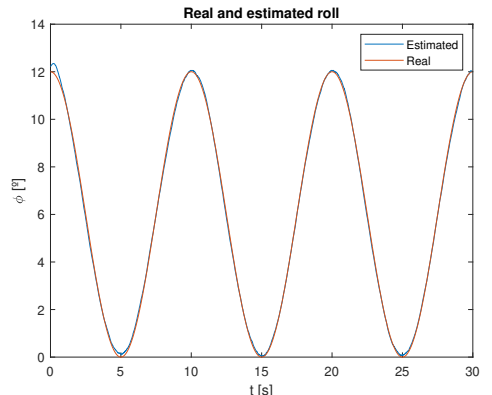
((b)) Rate gyro theoretical data.

Figure 13: Accelerometer and rate gyro data.

Figures 13(a) and 13(b) represent the data collected from the accelerometers and the gyroscope when the theoretical sine waves for pitch and roll were imposed.



((a)) Pitch.



((b)) Roll.

Figure 14: Comparison between estimated and simulated pitch and roll data.

Figures 14(a) and 14(b) superimpose the estimated and "real" (rather, simulated from the sinusoidal inputs) results for the pitch and roll angles, respectively. In both plots, the estimated and real signals are, to all extents, coincident, showing a good Euler angle estimation.

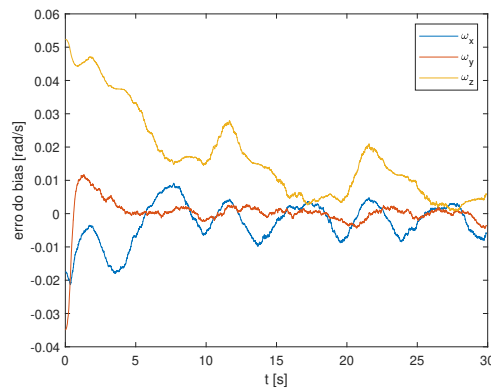


Figure 15: Rate gyro bias estimation error.

Figure 15 plots the bias estimation error for the gyroscope. Each individual bias tends to zero, with the biggest bias error measured at  $t = 0$  s being only 0.05 rad/s. As the bias estimation error is close to zero, the estimation of said bias is good.

Thus, figures 14 and 15 complete the validation of the Kalman filter in study, allowing for good estimates of both bias and Euler angles.

## 5.4 Experimental results

The implemented Kalman filter was then applied to the data obtained in experiment E. Figures 16(a) and 16(b) plot the accelerometer and rate gyro measurements for this experiment.

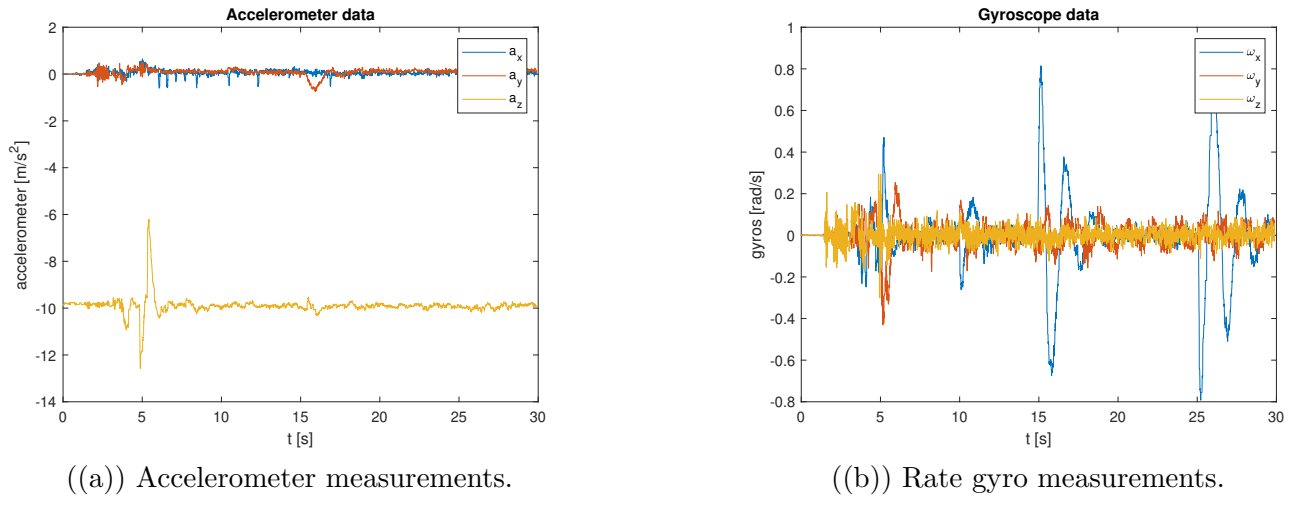


Figure 16: Accelerometer and rate gyro measurements.

For this section, the Q and R were defined as:  $Q = 0.004 \begin{bmatrix} I_{3 \times 3} & 0_{3 \times 3} \\ 0_{3 \times 3} & 0_{3 \times 3} \end{bmatrix}$ ,  $R = 0.008I_{3 \times 3}$

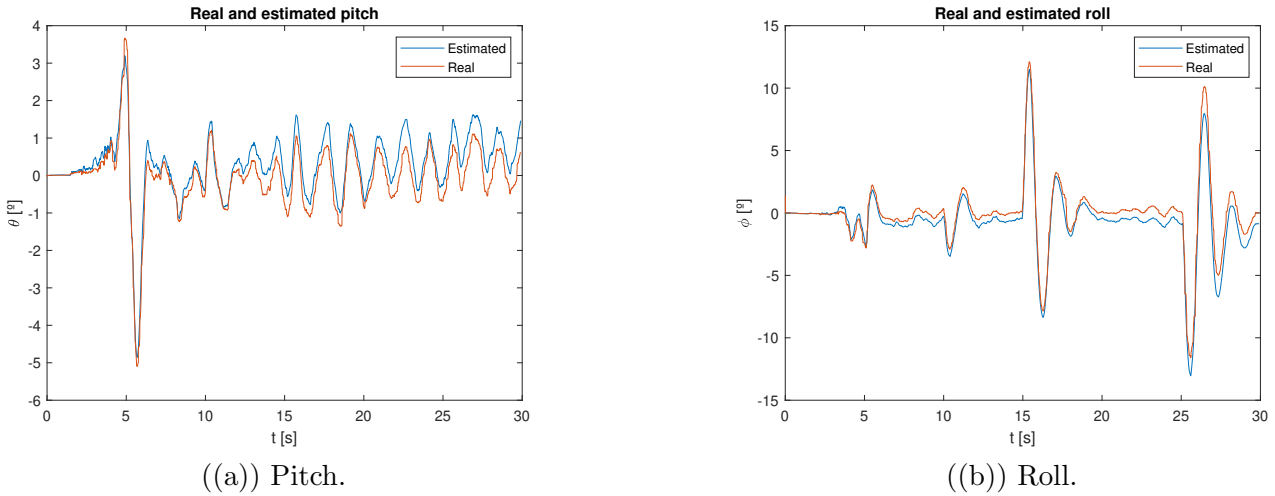


Figure 17: Comparison between reference and estimated experimental pitch and roll measurements.

Figures 17(a) and 17(b) overlay the reference pitch and roll angles, provided by the built-in drone estimator, with the estimated roll and pitch angle obtained with the Kalman filter. The results are similar, though a small offset is noticeable for both cases (the estimated pitch is, on average, bigger than the experimental pitch angle, and the reverse is verified for the roll angle).

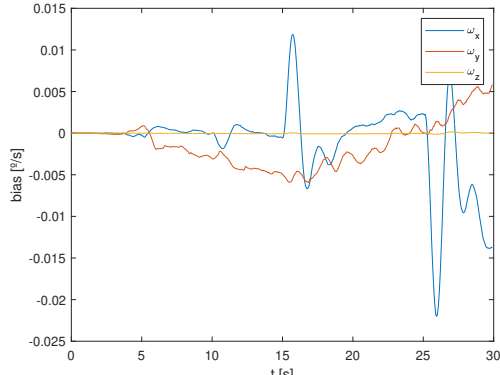


Figure 18: Estimated rate gyro bias.

Figure 18 plots the bias estimate. The bias estimate does not converge for  $\omega_x$  and  $\omega_y$ , while for  $\omega_z$  it remains at zero. A possible explanation could be that instead of two uncorrelated white Gaussian processes, the noise in the measurements could be correlated and coloured (i.e. not zero-mean), unlike what was tested in section 5.3, where the bias estimation error converged.

## 6 Conclusions

In this laboratory work, several different estimation solutions for the roll and pitch angles of the quadrotor were designed, implemented and studied.

This process began with the statistical characterisation of the motion variables measured in experiments *A*, *B* and *C*. This was done by computing the means and variances for each variables, in all the different test conditions, and interpreting their values in light of the different sources of disturbances in each test. These factors include the vibration introduced by the rotation of the electric motors, the instability of the hover condition of the quadcopter and even physical defects of the quadcopter used.

Having, at this point, a better knowledge of the quality of the measurements obtained in different test conditions, the focus shifted towards estimating the roll and pitch attitude of the quadcopter. The first approach considered was the direct computation of these angles from the components of the accelerometer measurements in each of the body axes. Preliminary results showed that this approach

was promising, despite being affected by significant high-frequency noise. However, a more detailed analysis revealed the presence of a constant bias in all of the estimations, a more serious limitation.

The next step was to develop a more complex estimation method, using a Kalman filter. This method had a much better capacity to smooth out the noise in the raw measurements, but was found to be heavily dependent on the estimate provided for the covariances  $Q$  and  $R$ , turning the tuning process into a very manual, trial-and-error process. The bias in the Kalman-provided estimate was reduced, when compared with the previous approach, but was still present (and found to be also strongly dependent on the values of  $Q$  and  $R$ ). This process was subsequently repeated, including an extra state with the objective of estimating also the bias of the rate gyro. This provided even better estimates than previously. Finally, an analysis of both of these approaches to filtering led to the conclusion that the filters thus obtained are complementary.

The last approach attempted was to estimate both the pitch and roll angles and the respective gyro biases through a single vector observation, following the methodology laid out in [1]. First, a simulation was carried out as proof-of-concept, using sinusoidal inputs with the objective of achieving an estimate for the Euler angles close to the theoretical results, as well as a bias estimation error close to zero so as to show the correct functioning of this solution. Then, it was applied to a real, experimental situation. These results were very satisfactory.

## References

- [1] P. Batista, C. Silvestre, and P. Oliveira. Partial attitude and rate gyro bias estimation: observability analysis, filter design, and performance evaluation. *International Journal of Control*, 84(2):895–903, 2011.
- [2] R. Cunha and J. Azinheira. *Estimation of Motion Variables of the Parrot AR.Drone*. 2022.
- [3] R. Cunha and J.R. Azinheira. *Sensors and State Estimation*. 2021.